Electronic Supplementary Material (ESI) for Chemical Communications.

Supporting information for

Geometrical control of the magnetic anisotropy in six coordinate cobalt complexes [**]

Mohamed R. Saber,[a,b] Mukesh K. Singh [a] and Kim R. Dunbar [a]*

[a] Department of Chemistry, Texas A&M University, College Station, Texas 77842-3012

[b] Department of Chemistry, Fayoum University, Fayoum 63514, Egypt.

RECEIVED DATE (automatically inserted by publisher); E-mail: dunbar@mail.chem.tamu.edu

---

[*] Prof. K. R. Dunbar, Dr. M. R. Saber, Dr. M. K. Singh
Department of Chemistry
Texas A&M University
College Station, TX 77842-3012 (USA)
Fax: (+1) 979-845-7177
E-mail: dunbar@mail.chem.tamu.edu

[**] K. R. D. gratefully acknowledges the National Science Foundation (CHE-1808779) and the Welch Foundation (A-1449) for financial support. We also thank the HPRC at Texas A&M University for the computing resources.

.

Table of Contents:

Experimental Section 3

  Syntheses 3

  X-ray Crystallographic Measurements 3

  Magnetic Measurements 3

Computational details 15

Table S1. Crystal structure data and refinement parameters for compounds **1** 4
Table S2. Selected bond distances (Å) and bond angles (°) for compound 1. 4
Table S 3. NEVPT2 transition energies of the ligand field states for 1 and its contributions to the *D* and *E* values. 16
Table S 4. NEVPT2 transition energies of the ligand field states for 2 and its contributions to the *D* and *E* values. 17

Figure S1. Molecular structure of $[Co(CH_3CN)_6](BF_4)_2$ (1). Thermal ellipsoids are drawn at the 50% probability level. Hydrogen atoms are omitted for the sake of clarity. 5
Figure S 2. χT versus T plot for 1. The solid line represents the fit using PHI. 6
Figure S 3. Field dependence of the magnetization data for 1 at 2K. What is the line? 6
Figure S 4. Reduced magnetization data for 1 from 1.8-4.5 K. 7
Figure S 5. Temperature dependence of the in-phase (χ’) and out-of-phase (χ”) AC signals for 1. 8
Figure S 6. Field dependence of the out-of-phase (χ”) AC signals for 1. 8
Figure S 7. Frequency dependence of the in-phase (χ’) and out-of-phase (χ”) AC signals for 1 under a 1500 Oe applied dc field. 9
Figure S 8. Cole-Cole plot (top) and Arrhenius plot (bottom) for 2. Solid line represents fit using the Debye model. 10
Figure S 9. χT versus T plot for 2. Solid line represents fit using PHI (top). Inset: Reduced magnetization data for 2 at 1.8-4.5K. Field dependence of the magnetization for 2 at 2K (bottom). WHAT IS THE LINE? 11
Figure S 10. Temperature dependence of the in-phase (χ’) and out-of-phase (χ”) AC signals for 2. 12
Figure S 11. Field dependence of the out-of-phase (χ”) AC signals for 2. 12
Figure S 12. Frequency dependence of the in-phase (χ’) and out-of-phase (χ”) AC signals for 1 under a zero applied field (left) and a 2000 Oe applied dc field (right). 13
Figure S 13. Cole-Cole plots for 1 under a zero applied field (left) and a 2000 Oe applied dc field (right). 13
Figure S 14. Arrhenius fit (top) and hysteresis loops for 2. 14
Figure **S 15.** Multi-determinant characteristics of the ground and excited states wave function for **1** (left) and **2** (right). Only computed CI coefficients that are larger than 10% are shown. 18
Figure **S 16.** *Ab initio* NEVPT2+SA-CASSCF computed energy levels for all roots for **1** and **2**. Black = quartet energy levels and red = doublet energy levels. Spin flip energy states i.e. doublets, are higher in energy indicating less contribution to anisotropy parameters from spin flip transitions. 19

Experimental Section

Syntheses

Starting Materials. All chemicals and solvents are of reagent grade quality. The KTp^{py} ligand was synthesized according to the reported procedure.[1] Acetonitrile and CH_2Cl_2 were pre-dried over 4 Å molecular sieves and freshly distilled under a nitrogen atmosphere.

[Co(MeCN)$_6$](BF$_4$)$_2$ (1). The compound was synthesized as follows: $NOBF_4$ (500 mg, 4.32 mmol) was mixed with excess cobalt powder in acetonitrile. The reaction was stirred overnight, filtered and diffused with diethyl ether which resulted in orange crystals suitable for X-ray measurements. (Yield = 895 mg, 87%). Elemental analysis: Calcd. for $C_{12}H_{18}CoF_8N_6B_2$ (**1**): C, 30.10; H, 3.79; N, 17.55; Found: C, 29.93; H, 3.76; N, 17.51.

[CoTp^{py}]PF$_6$ (2). The compound was synthesized following the reported procedure[2] as follows: A solution of cobalt(II) acetate (124 mg, 0.5 mmol) and KTp^{py} (242 mg, 0.5 mmol) in 10 mL of CH_3OH was mixed to give a pink solution. A 10 mL aliquot of KPF_6 (300 mg) in water was added to yield a pale pink precipitate which was collected by filtration, washed with water and dried under vacuum. The sample was recrystallized from CH_2Cl_2/hexanes (Yield = 205 mg, 63%). Elemental analysis: Calcd. for $C_{24}H_{19}BCoF_6N_9P$ (**2**): C, 44.47; H, 2.95; N, 19.45; Found: C, 44.31; H, 2.76; N, 19.55.

X-ray Crystallographic Measurements

X-ray diffraction data for **1** were collected at 110 K on a Bruker D8-QUEST diffractometer equipped with a IµS Mo microsource (λ = 0.71073 Å). The data were corrected for absorption using SADABS-2014/5.[3] The space group was determined from analysis of the systematic absences and E-statistics using XPREP. The structures were solved using the intrinsic phasing routine in SHELXT.[4] The nonhydrogen atoms were located from the difference Fourier map and refined using a least-squares refinement algorithm in SHELXL-2014.[4] All non-hydrogen atoms were refined anisotropically and all hydrogen atoms were placed in calculated positions and refined with thermal parameters constrained to their parent atom. Molecular graphics were produced using Diamond.[5] Table S1 contains a summary of the crystal and refinement data.

Magnetic Measurements

DC magnetic measurements were performed on freshly prepared crushed crystalline samples in plastic bags over the temperature range of 2–300 K in an applied magnetic field of 1000 Oe on a Quantum Design SQUID, Model MPMS equipped with a 7 Tesla magnet. The diamagnetic contribution of the polypropylene bag was subtracted from the raw data. Pascal's constants[6] were used to estimate the diamagnetic corrections, which were subtracted from the experimental susceptibilities to give the molar paramagnetic susceptibilities (χ_M). AC magnetic susceptibility measurements were performed on the same samples with an oscillating field of 3 Oe in the range of 1-1500 Hz.

Table S1. Crystal structure data and refinement parameters for compound **1**

Compound	**1**
Empirical formula	$C_{12}H_{18}B_2CoF_8N_6$
Formula weight	478.87
Temperature/K	110
Crystal system	monoclinic
Space group	$P2_1/n$
a/Å	5.8051(4)
b/Å	17.7416(11)
c/Å	22.0260(14)
α/°	90
β/°	90.256(2)
γ/°	90
Volume/Å^3	2268.5(3)
Z	4
ρ_{calc}g/cm^3	1.402
μ/mm^{-1}	0.829
F(000)	964
Crystal size/mm^3	0.23 × 0.1 × 0.1
Radiation	MoKα (λ = 0.71073)
2Θ range for data collection/°	4.354 to 54.204
Index ranges	$-7 \le h \le 7$, $-22 \le k \le 22$, $-28 \le l \le 28$
Reflections collected	30008
Independent reflections	4992 [R_{int} = 0.0626, R_{sigma} = 0.0432]
Data/restraints/parameters	4992/0/268
Goodness-of-fit on F^2	1.25
Final R indexes [I>=2σ (I)]	R_1 = 0.0834, wR_2 = 0.1559
Final R indexes [all data]	R_1 = 0.1084, wR_2 = 0.1646
Largest diff. peak/hole / e Å^{-3}	0.66/-0.38

[a] $R_1 = \Sigma||F_o| / |F_c||\Sigma|F_o|$. [b] $wR_2 = [\Sigma[w(F_o^2 - F_c^2)^2]/\Sigma[w(F_o^2)^2]]^{1/2}$

Table S2. Selected bond distances (Å) and bond angles (°) for compound **1.**

$[Co(CH_3CN)_6](BF_4)_2$ **(1)**			
Co1- N1	2.126(4)	N(1)-Co-N(2)	91.99(5)
Co1- N2	2.123(4)	N(1)-Co-N(3)	91.06(5)
Co1- N5	2.105(4)	N(2)-CO-N(3)	93.26(5)
Co1- N6	2.119(4)	N(1)-CO-N(4)	89.02(5)
Co1- N3	2.104(4)	N(1)-Co-N(5)	87.75(5)
Co1- N4	2.102(4)	N(2)-Co-N(4)	87.42(5)
		N(2)-Co-N(6)	87.79(5)
		N(3)-Co-N(5)	89.09(5)

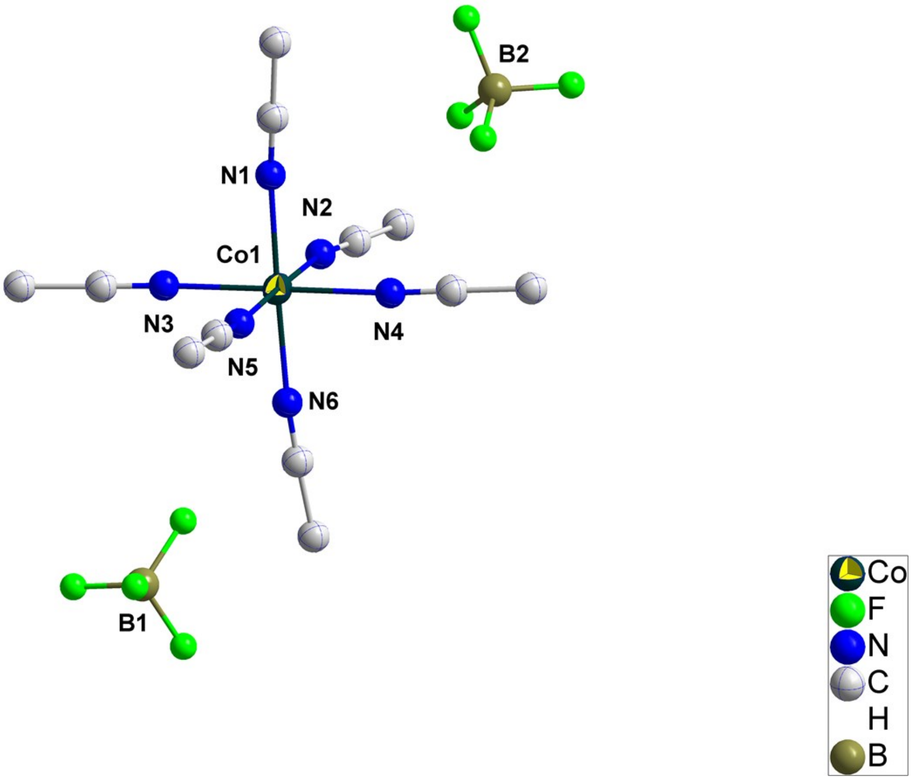

Figure S1. Molecular structure of $[Co(CH_3CN)_6](BF_4)_2$ (**1**). Thermal ellipsoids are drawn at the 50% probability level. Hydrogen atoms are omitted for the sake of clarity.

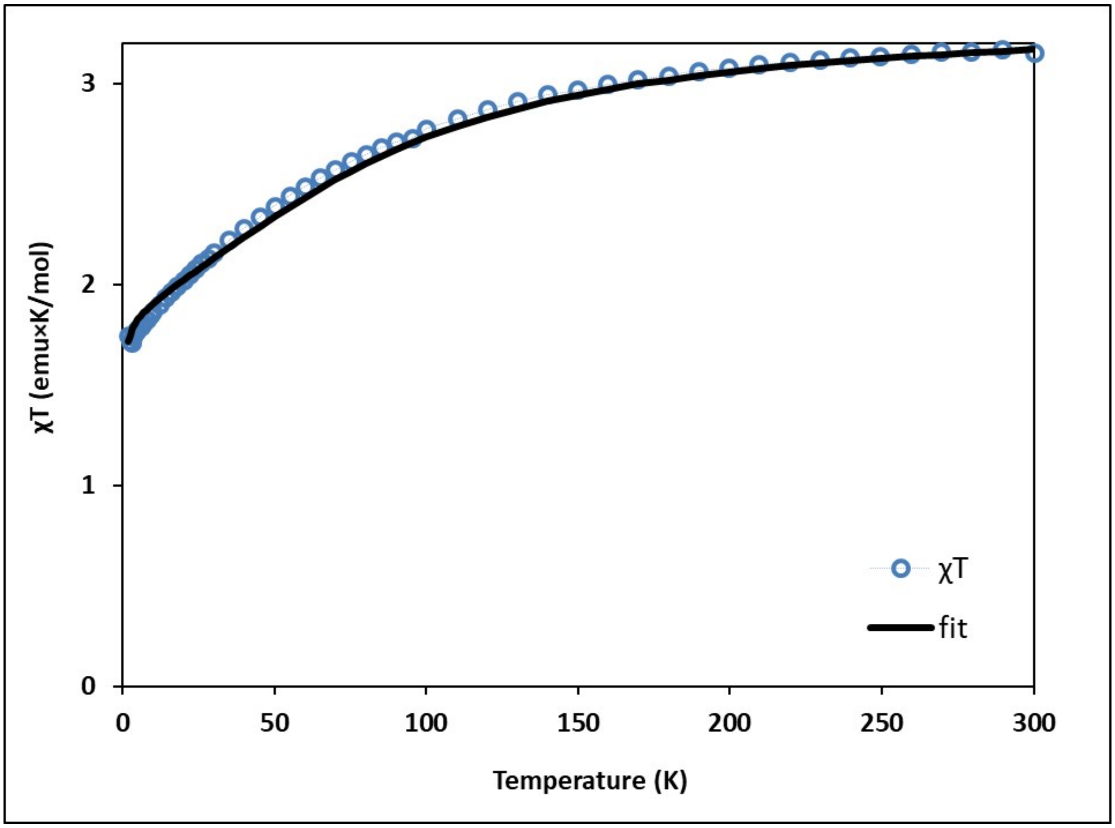

Figure S 2. χT versus T plot for **1**. The solid line represents the fit using PHI.

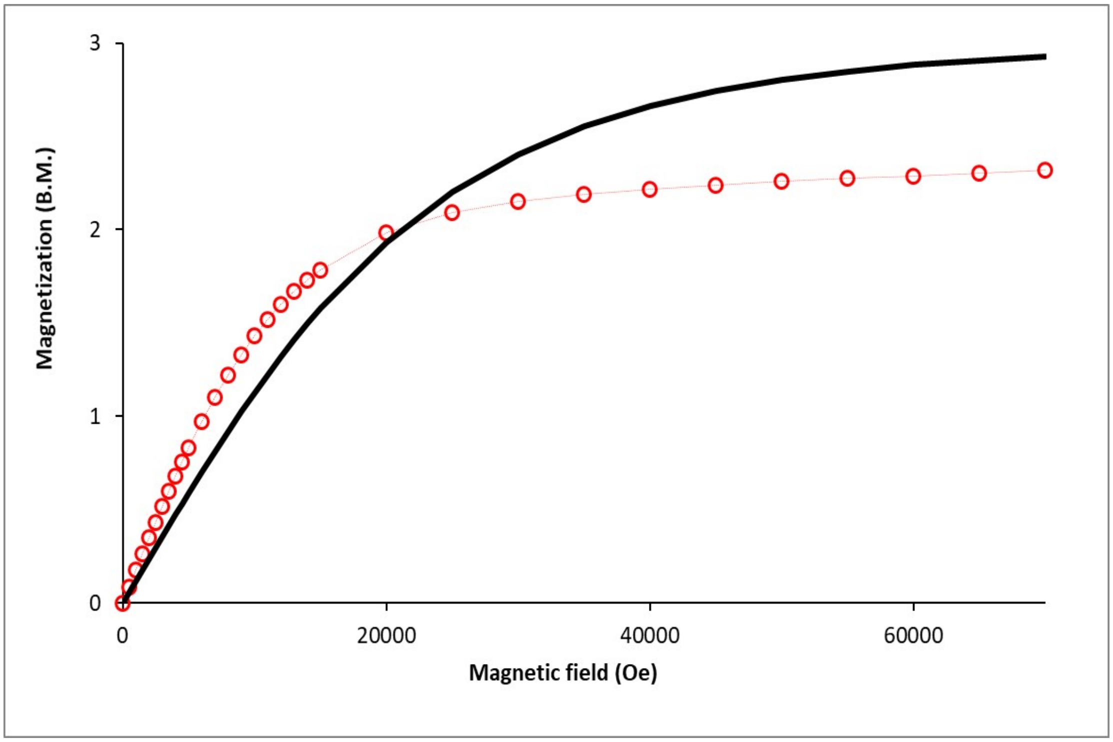

Figure S 3. Field dependence of the magnetization data for **1** at 2K. Solid line represents Brillouin function for S = 3/2, g = 2.

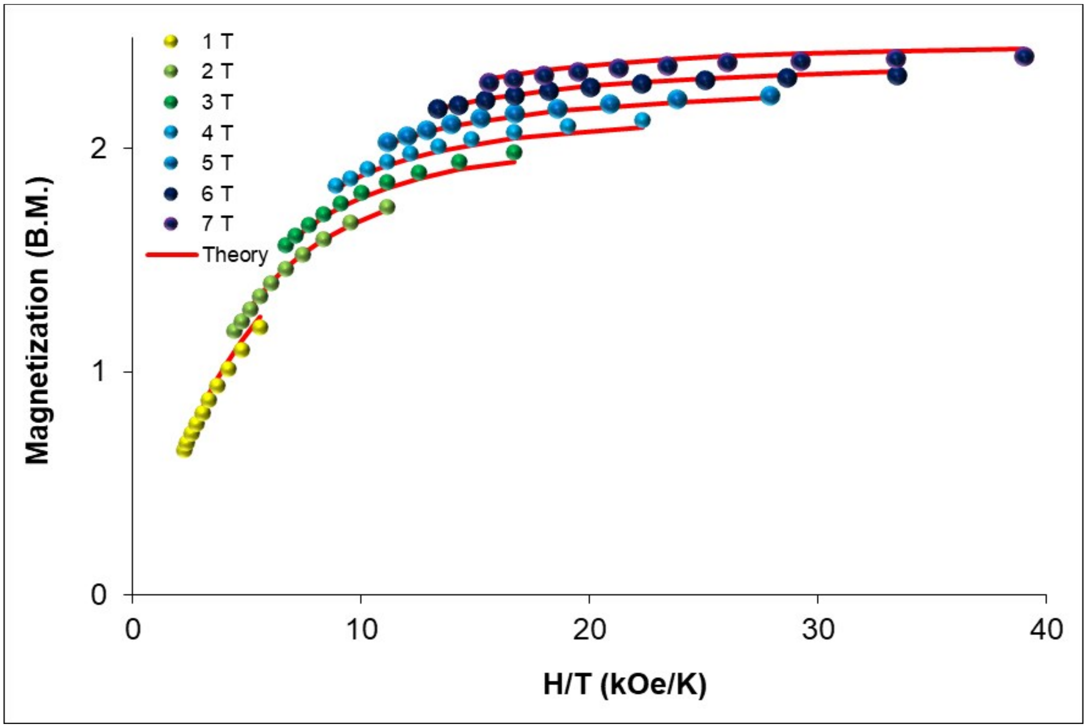

Figure S 4. Reduced magnetization data for **1** from 1.8-4.5 K. solid lines represent fits using ANISOFIT2 (g = 2.45, D = +40.5 cm^{-1} , E = 5.86 cm^{-1}).

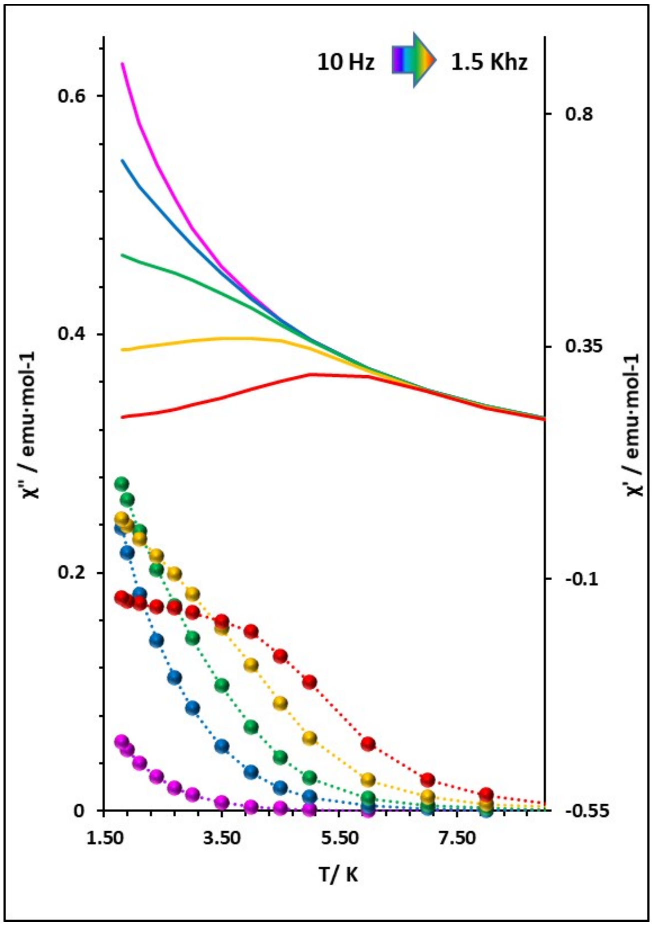

Figure S 5. Temperature dependence of the in-phase (χ’) and out-of-phase (χ”) AC signals for **1**.

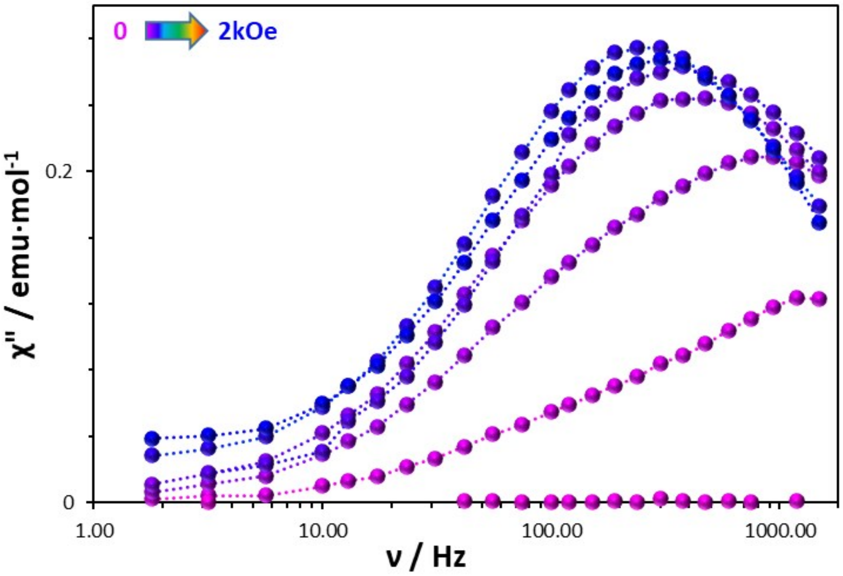

Figure S 6. Field dependence of the out-of-phase (χ”) AC signals for **1**.

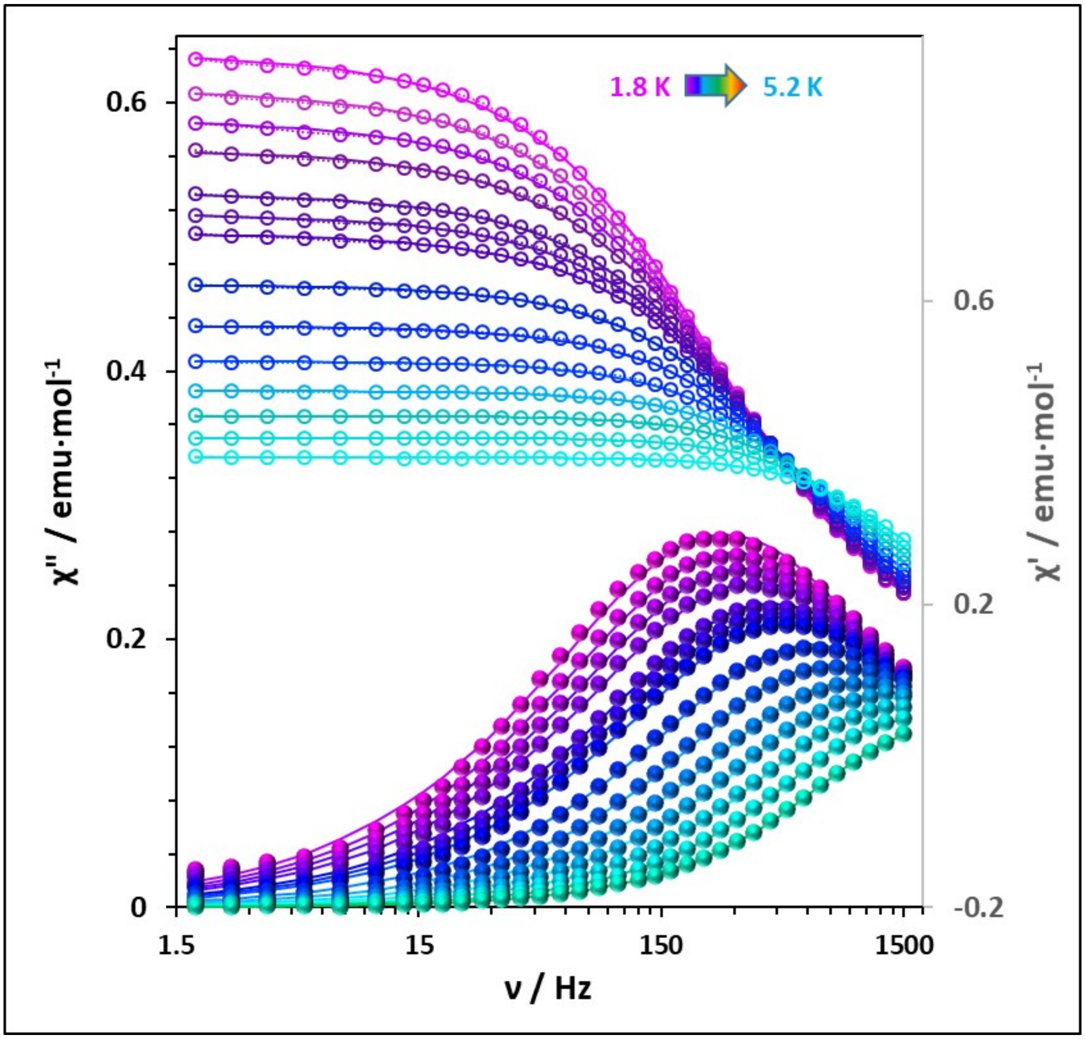

Figure S 7. Frequency dependence of the in-phase (χ’) and out-of-phase (χ”) AC signals for **1** under a 1500 Oe applied dc field.

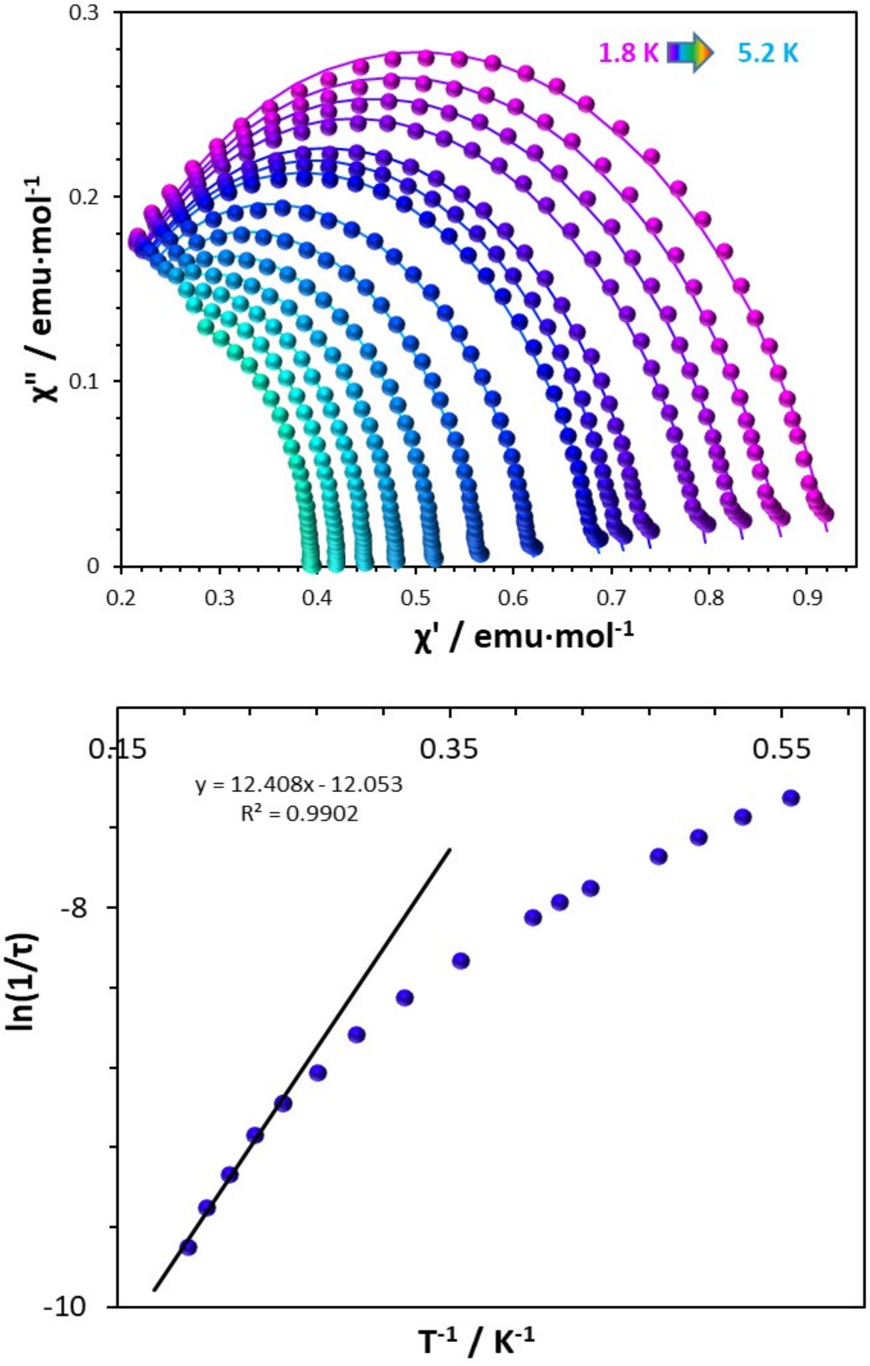

Figure S 8. Cole-Cole plot (top) and Arrhenius plot (bottom) for **1**. Solid line represents fit using the Debye model.

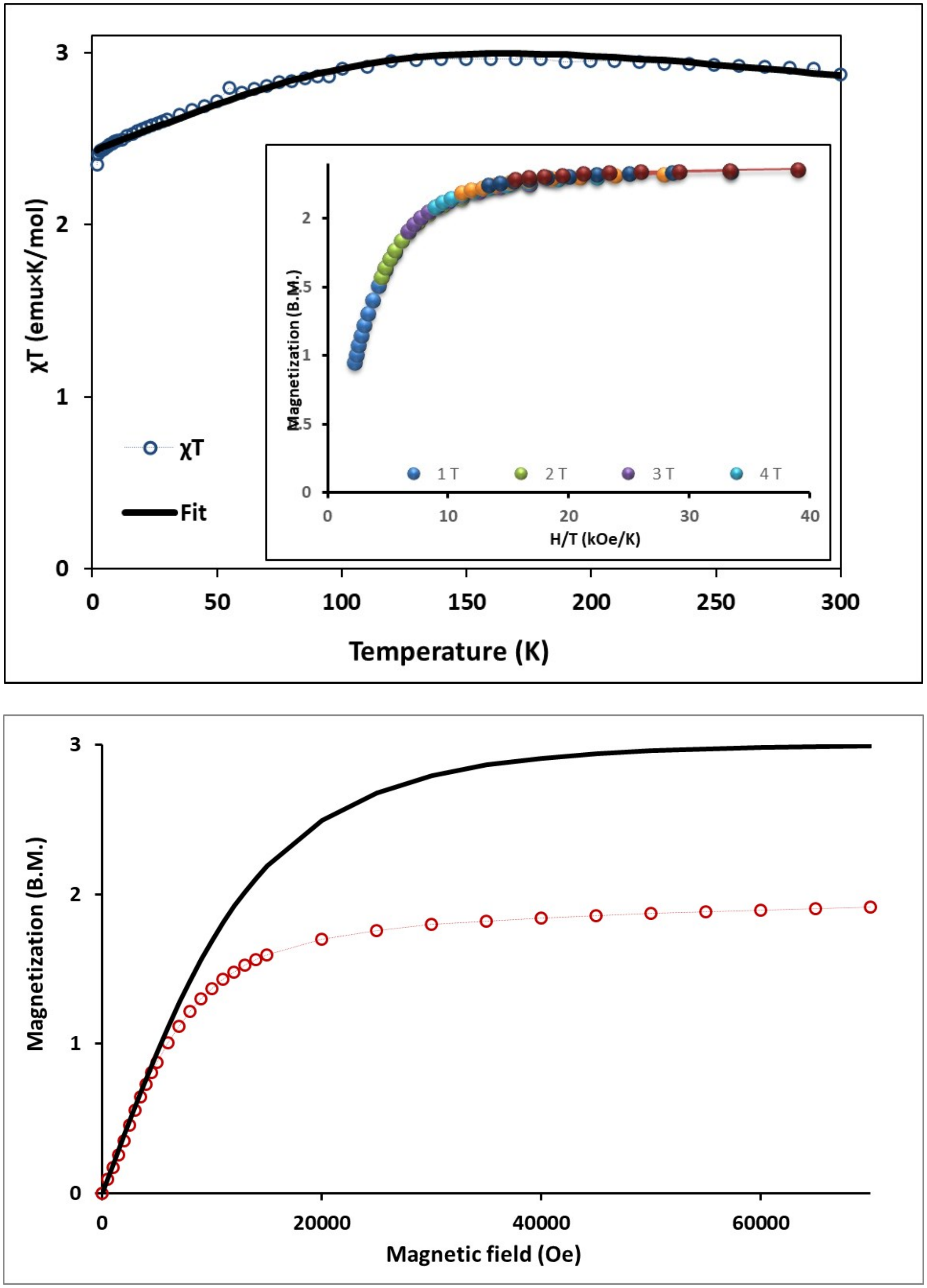

Figure S 9. χT versus T plot for **2**. Solid line represents fit using PHI (top). Inset: Reduced magnetization data for **2** at 1.8-4.5K (solid lines are fits using ANISOFIT2, g = 3.01, D = -189 cm^{-1}, E = 10.4 cm^{-1}). Field dependence of the magnetization for **2** at 2K (bottom). Solid line represents Brillouin function for S = 3/2, g = 2.

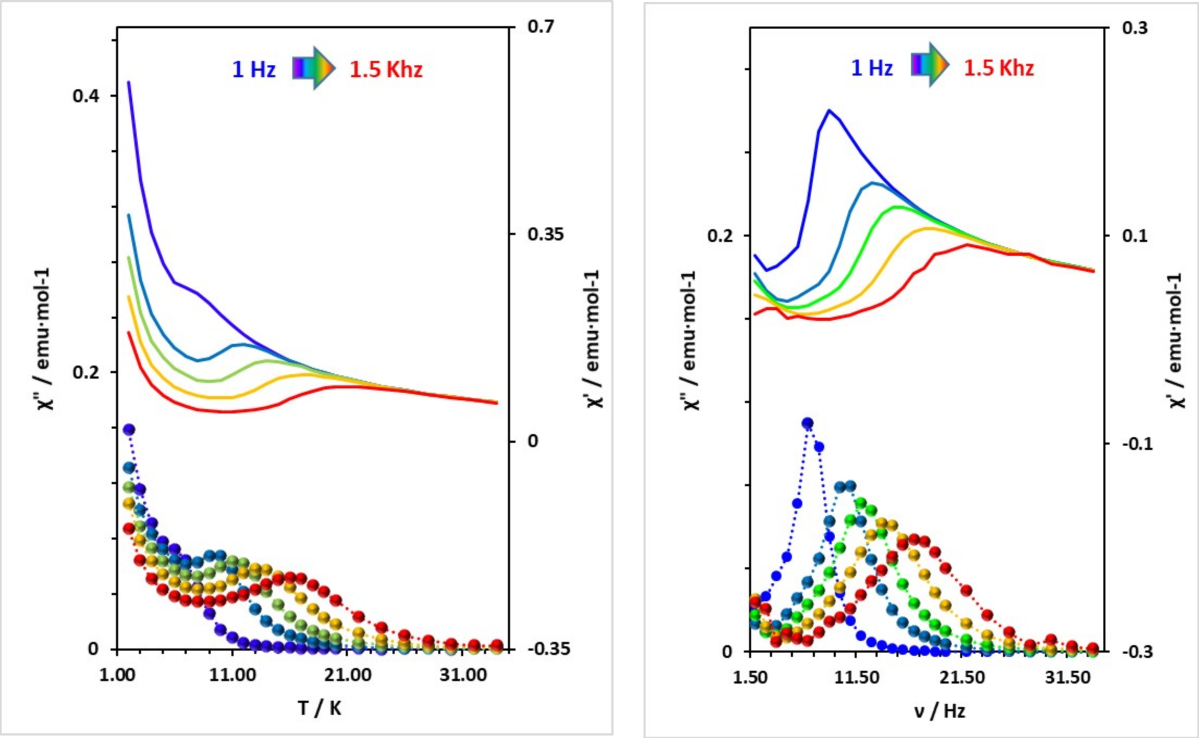

Figure S 10. Temperature dependence of the in-phase (χ') and out-of-phase (χ'') AC signals for **2.**

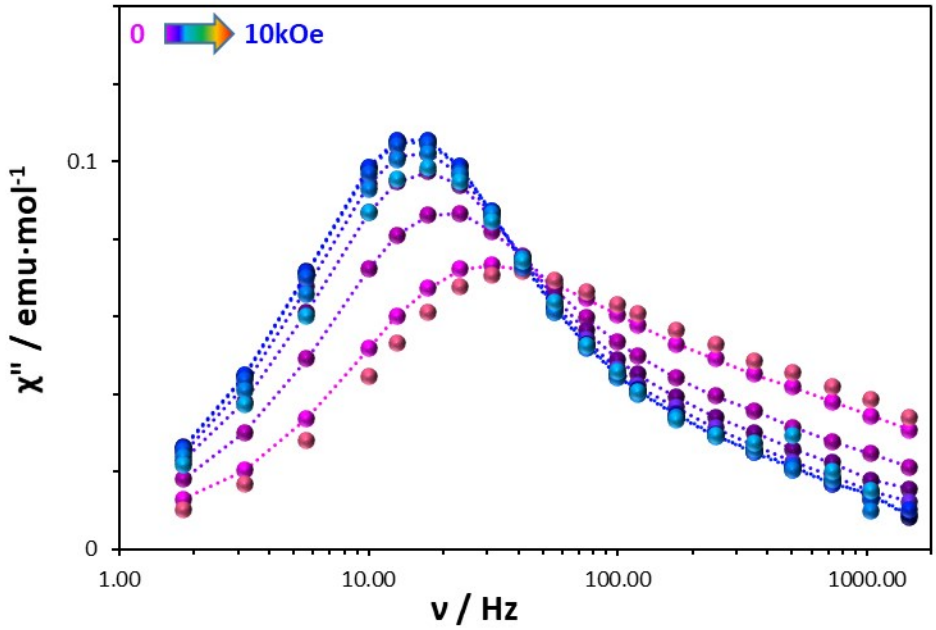

Figure S 11. Field dependence of the out-of-phase (χ'') AC signals for **2**.

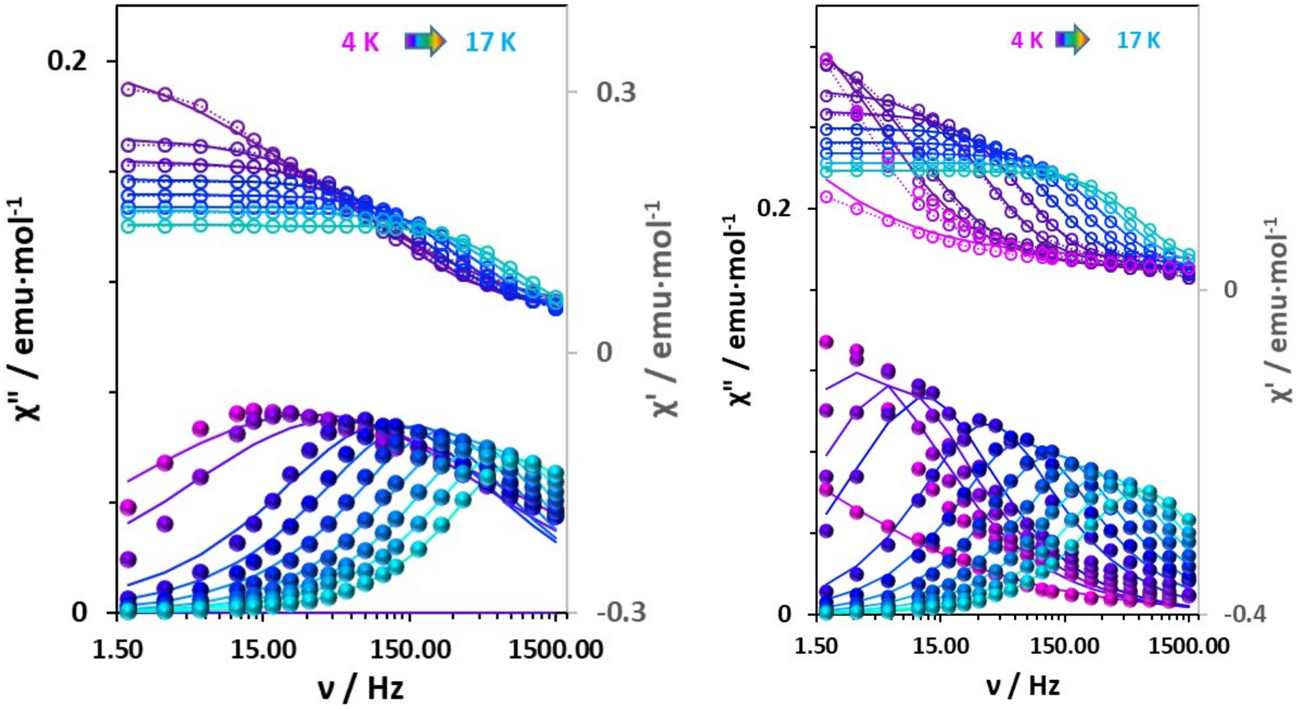

Figure S 12. Frequency dependence of the in-phase (χ’) and out-of-phase (χ”) AC signals for **1** under a zero applied field (left) and a 2000 Oe applied dc field (right).

Figure S 13. Cole-Cole plots for **1** under a zero applied field (left) and a 2000 Oe applied dc field (right).

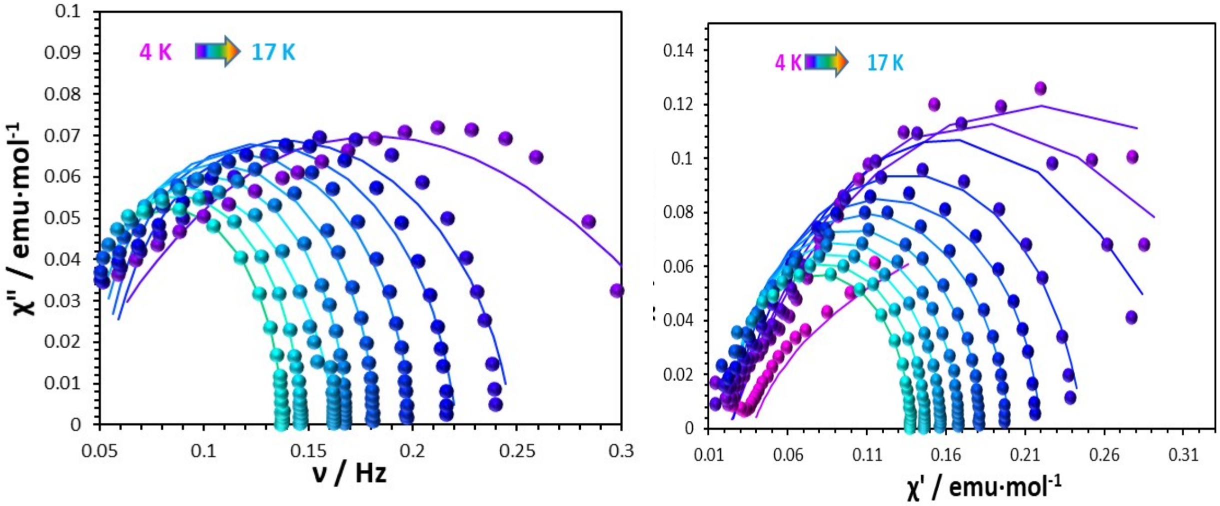

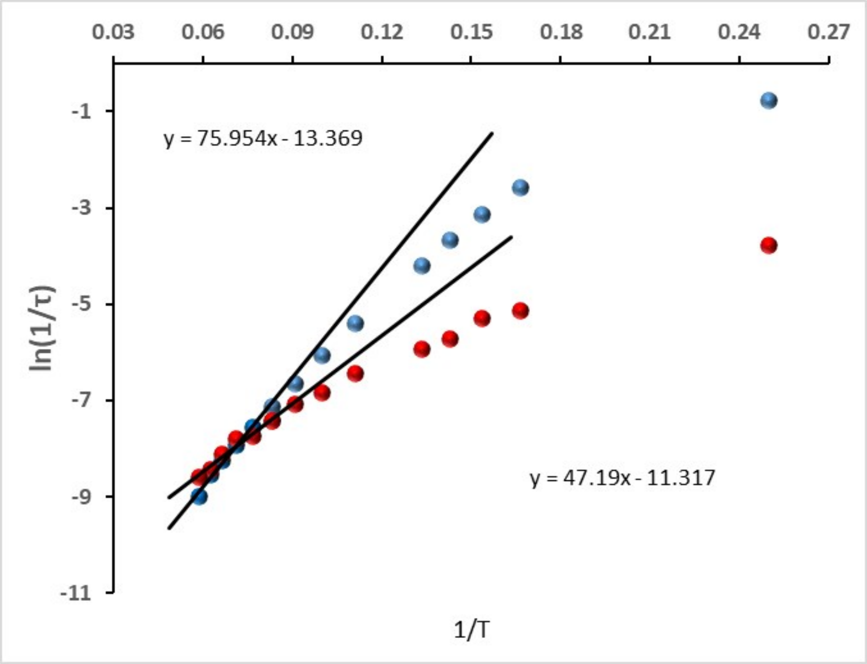

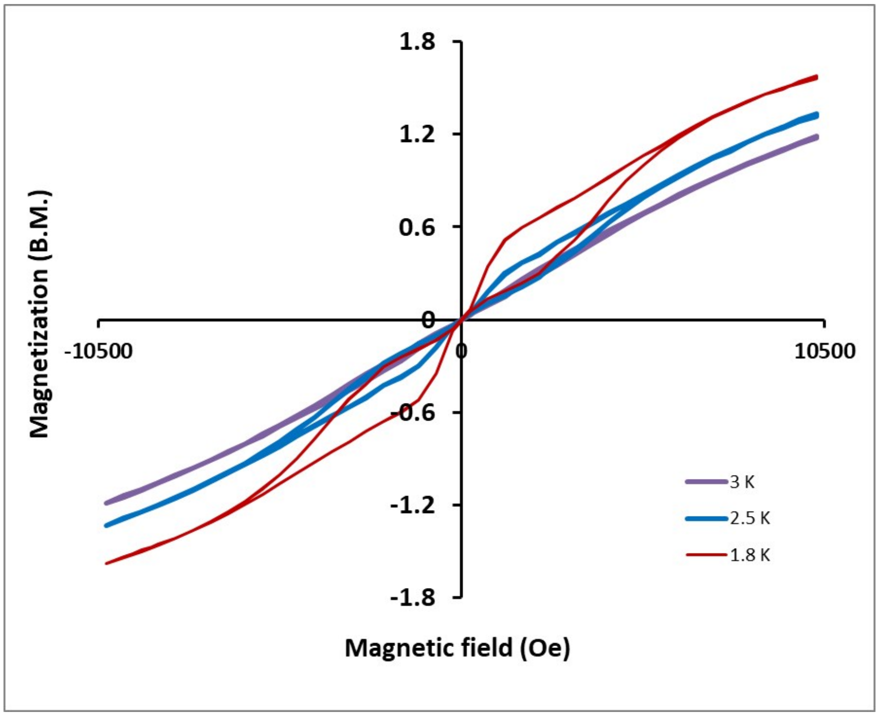

Figure S 14. Arrhenius fit (top) and hysteresis loops for **2**.

Computational details

The *ab initio* calculations on the XRD structures were performed in the ORCA software suite (version ORCA 4.1.0) to estimate ZFS parameters for **1**-**2**.[7] The scalar relativistic Hamiltonian was considered by using the zeroth-order regular approximation (ZORA) method. Furthermore, ZORA contracted versions of basis sets ZORA-def2-TZVPP were used for Co and the ZORA-def2-TZVP basis set was used for the rest of the atoms. State-average complete active space self-consistent field (SA-CASSCF) calculations were performed with five d-orbitals and seven electrons (CAS (7,5) setup) in the active space. Ten quartet and forty doublet roots were used in the calculations[8]. The 2nd order N-electron valence perturbation theory (NEVPT2) calculation, which takes dynamic correlation into account, is known to give accurate estimations of the ZFS parameters. We have restricted our analysis to NEVPT2 results.

We also performed CASSCF calculations using the MOLCAS 8 code to estimate anisotropy parameters. Here we employed the [ANO-RCC-VTZP] basis set for the Co atom, the [ANO-RCC-VDZP] basis set for N atoms, and the [ANO-RCC-VDZ] basis set for C and H atoms. CASSCF calculations were performed using seven electrons in the five active orbitals with an active space of CAS(7,5). We computed 10 quartets and 40 doublets using the configuration interaction (CI) procedure and then performed the RASSI-SO module to compute the spin-orbit coupled states. After computing these SO states, we performed the SINGLE_ANISO code to extract the corresponding anisotropy parameters.

Table S 3. NEVPT2 transition energies of the ligand field states for **1** and its contributions to B_2^0.

B_2^0 = 146.5 cm^{-1}

g_{xx}, g_{yy}, g_{zz} = 1.741, 2.562, 2.563

NEVPT2 energy levels cm^{-1}	Multiplicity	Root	Contribution to B_2^0
0.0	4	0	0.0
187.1	4	1	57.6
187.6	4	2	57.6
9953.0	4	3	1.8
9953.0	4	4	1.8
9981.0	4	5	-14.7
20892.0	4	6	0.0
22535.2	4	7	0.1
22538.1	4	8	0.1
22714.5	4	9	0.0
8797.5	2	0	-3.8
8797.5	2	1	-3.8
17744.0	2	2	0.0
17817.2	2	3	-1.3
17817.2	2	4	-1.3
18477.8	2	5	0.0
18478.0	2	6	0.0
18576.8	2	7	0.0
22246.8	2	8	2.9
22254.8	2	9	0.0
22254.8	2	10	-0.1
26006.1	2	11	-0.1
28195.6	2	12	0.9
28378.2	2	13	-0.1
28378.2	2	14	-0.1
29669.4	2	15	-0.3
29669.5	2	16	-0.3
29725.5	2	17	0.0
31675.3	2	18	-0.7
31675.4	2	19	-0.7
35217.1	2	20	1.4
35269.4	2	21	-0.2
35269.4	2	22	-0.2
36932.5	2	23	-0.1
36932.6	2	24	-0.1
37163.1	2	25	0.0
38156.5	2	26	-0.2
38156.6	2	27	-0.2
41239.9	2	28	0.4
41366.0	2	29	0.0
41366.1	2	30	0.0
44425.9	2	31	0.0
44587.5	2	32	-0.1
44651.0	2	33	-0.1
44651.1	2	34	0.0
64517.1	2	35	-0.1
64517.3	2	36	-0.1
65315.8	2	37	0.0
65317.6	2	38	0.0
65575.7	2	39	0.0

Table S 4. NEVPT2 transition energies of the ligand field states for **2** and its contributions to B_2^0.

B_2^0 = -150.6 cm^{-1}

g_{xx}, g_{yy}, g_{zz} = 1.352, 1.356, 3.513

NEVPT2 energy levels cm^{-1}	Multiplicity	Root	Contribution to B_2^0
0.0	4	0	0.0
25.6	4	1	-169.1
8574.1	4	2	2.2
8576.3	4	3	5.4
8649.1	4	4	3.5
9794.9	4	5	2.1
12165.3	4	6	0.3
22169.2	4	7	0.0
22219.2	4	8	0.0
22332.8	4	9	0.0
14862.9	2	0	-0.5
14980.3	2	1	-0.1
18060.1	2	2	0.8
18092.5	2	3	0.2
18509.4	2	4	0.0
18606.1	2	5	0.0
18646.6	2	6	5.6
22336.4	2	7	-1.0
23573.1	2	8	-1.7
23775.6	2	9	-0.8
23790.6	2	10	1.0
24882.1	2	11	0.5
26885.2	2	12	0.1
26912.7	2	13	0.1
27752.0	2	14	0.1
28338.5	2	15	0.0
28343.3	2	16	0.0
28831.3	2	17	-0.2
28866.8	2	18	-0.2
30103.0	2	19	0.0
30319.6	2	20	0.0
31199.2	2	21	-1.1
31230.0	2	22	-1.1
33905.5	2	23	0.0
35954.3	2	24	0.0
35955.2	2	25	0.0
36987.1	2	26	0.1
37007.6	2	27	0.0
40299.6	2	28	0.1
40308.5	2	29	0.3
41867.0	2	30	-0.1
41933.7	2	31	-0.1
42851.0	2	32	-0.1
43015.2	2	33	-0.1
45218.4	2	34	0.0
60260.9	2	35	0.0
62553.5	2	36	0.0
62674.2	2	37	0.0
64778.5	2	38	0.0
64791.5	2	39	0.1

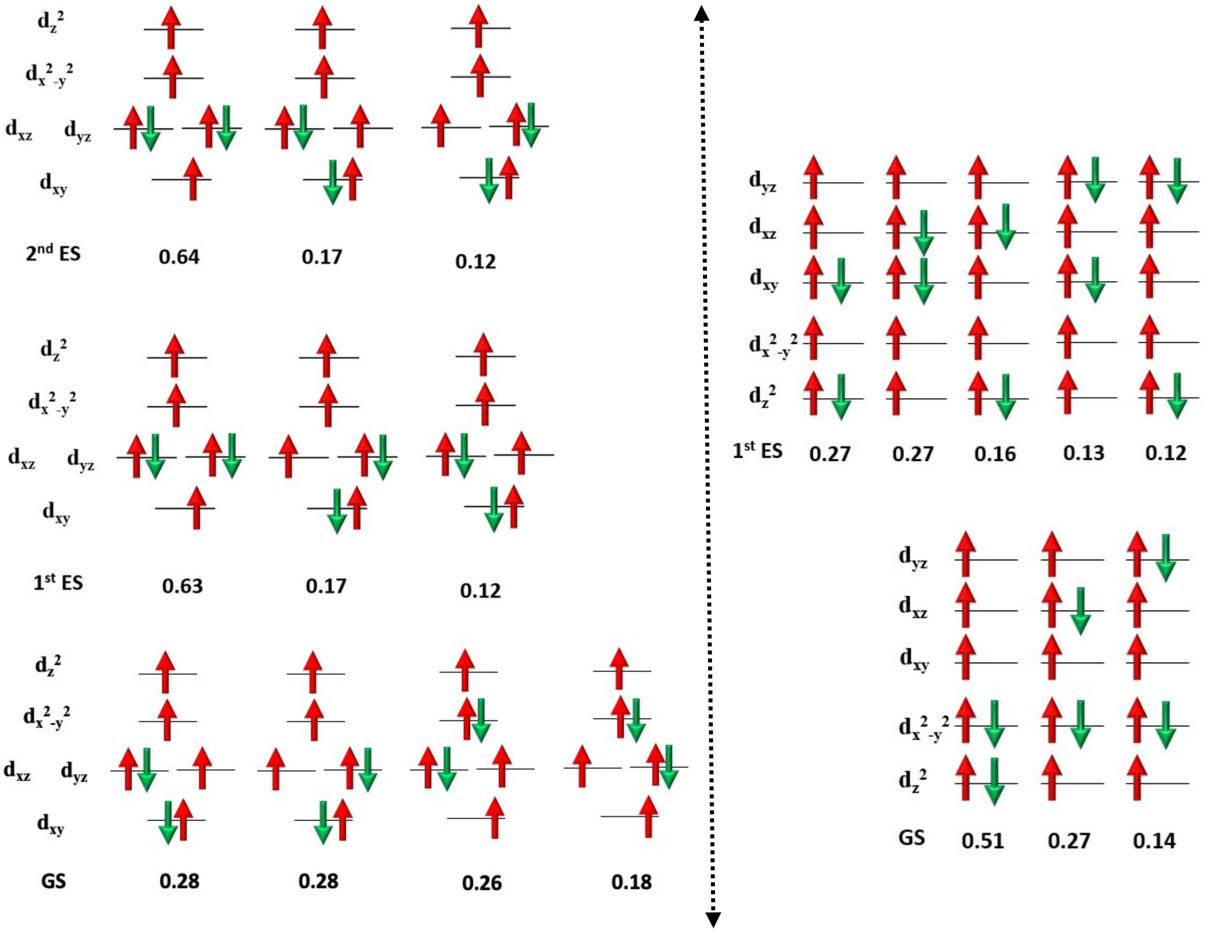

Figure **S 15.** Multi-determinant characteristics of the ground and excited states wave function for **1** (left) and **2** (right). Only computed CI coefficients that are larger than 10% are shown.

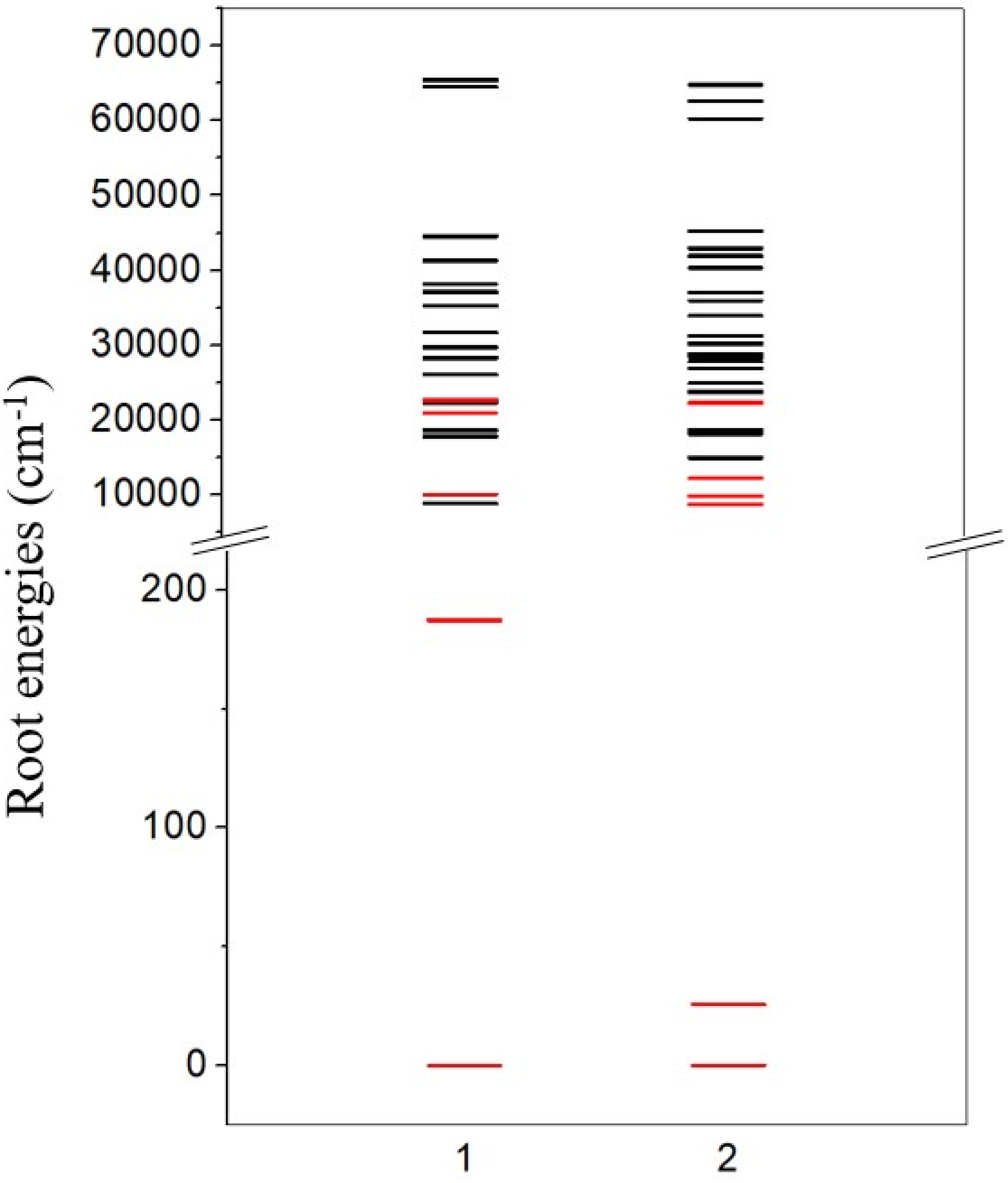

Figure **S 16.** *Ab initio* NEVPT2+SA-CASSCF computed energy levels for all roots for **1** and **2**. Red = quartet energy levels and black = doublet energy levels. Spin flip energy states i.e. doublets, are higher in energy indicating less contribution to anisotropy parameters from spin flip transitions.

1. P. L. Jones, A. J. Amoroso, J. C. Jeffery, J. A. McCleverty, E. Psillakis, L. H. Rees and M. D. Ward, *Inorg. Chem.*, 1997, **36**, 10-18.
2. R. L. Paul, A. J. Amoroso, P. L. Jones, S. M. Couchman, Z. R. Reeves, L. H. Rees, J. C. Jeffery, J. A. McCleverty and M. D. Ward, *J. Chem. Soc., Dalton Trans.*, 1999, DOI: 10.1039/A900805E, 1563-1568.
3. G. M. Sheldrick., in *SADABS: A program for absorption correction with the Bruker SMART system*, University of Göttingen, Germany, 2008.
4. G. M. Sheldrick, *Acta Crystallogr. Sec. A*, 2008, **64**, 112-122.
5. W. Pennington, *J. Appl. Crystallogr.*, 1999, **32**, 1028-1029.
6. G. A. Bain and J. F. Berry, *J. Chem. Educ.*, 2008, **85**, 532.
7. F. Neese, *WIREs Comput. Mol. Sci.*, 2012, **2**, 73.
8. R. Herchel, L. Vahovska, I. Potocnak and Z. Travnicek, *Inorg. Chem.*, 2014, **53**, 5896-5898.